

Nanoscale metallic iron for environmental remediation: prospects and limitations

Chicgoua Noubactep^{(a,d),*}, Sabine Caré^(b), Richard Crane^(c)

^(a) Angewandte Geologie, Universität Göttingen, Goldschmidtstraße 3, D - 37077 Göttingen, Germany.

^(b) Université Paris-Est, Laboratoire Navier, (ENPC/IFSTTAR/CNRS), 2 allée Kepler, 77420 Champs sur Marne, France.

^(c) Interface Analysis Centre, University of Bristol, 121 St. Michael's Hill, Bristol, BS2 8BS, UK.

^(d) Kultur und Nachhaltige Entwicklung CDD e.V., Postfach 1502, D - 37005 Göttingen, Germany.

Correspond author; e-mail: cnoubac@gwdg.de; Tel. +49 551 39 3191, Fax. +49 551 399379

Abstract

The amendment of the subsurface with nanoscale metallic iron particles (nano-Fe⁰) has been discussed in the literature as an efficient in-situ technology for groundwater remediation. However, the introduction of this technology was controversial and its efficiency has never been univocally established. This unsatisfying situation has motivated this communication whose objective was a comprehensive discussion of the intrinsic reactivity of nano-Fe⁰ based on the state-of-the art knowledge on the mechanism of contaminant removal by Fe⁰ and a mathematical modelling. It is showed that due to limitations of the mass transfer of nano-Fe⁰ to contaminants, available concepts can not explain the success of nano-Fe⁰ injection for in-situ groundwater remediation. It is recommended to test the possibility of introducing nano-Fe⁰ to initiate the formation of roll-fronts which propagation would induce the reductive transformation of both dissolved and adsorbed contaminants. Within a roll-front, Fe^{II} from nano-Fe⁰ is the reducing agent for contaminants. Fe^{II} is recycled by biotic or abiotic Fe^{III} reduction. While the roll-front concept could explain the success of already implemented reaction zones, more research is needed for a science-based recommendation of nano-Fe⁰ for subsurface treatment by roll-fronts.

Keywords: Environmental remediation, Material reactivity, Nanoscale iron, Roll-front, Zerovalent iron.

1 Introduction

The development of new methods and materials for environmental remediation is a real challenge for the scientific community. Such technologies will only be adopted by industry if they can exhibit marked improvements in efficiency, affordability or eco-compatibility compared to conventional techniques. The use of metallic iron (Fe^0) in subsurface reactive permeable barriers has been identified as such a technology [1-4]. Since this discovery almost 20 years ago, extensive research of $\text{Fe}^0/\text{H}_2\text{O}$ system has been performed in an attempt to understand the controlling mechanisms behind the remediation of redox-amenable contaminant species using Fe^0 -based materials [5-14]. Two different tools are commonly used to optimise the efficiency of Fe^0 for aqueous contaminant removal: (i) reducing the particle size of Fe^0 down to the nanoscale (nano- Fe^0) [15,16], and (ii) using bimetallic systems [17,18]. In recent years there has been considerable interest into combining the two methods [19-23].

Since the original proof of concept study into the application of nano- Fe^0 for water treatment at Lehigh University, USA [15], research within this field has boomed. On April 23th 2011, a search at “**Science Direct**” using key words “*nanoscale*” and “*zerovalent iron*” yielded 208 peer-reviewed articles in 6 selected journals (Table 1). The same search at “**Environmental Science and Technology**” resulted in 157 articles. According to Table 1, 59 articles have already been published in the first quarter of 2011 in the 7 selected journals. This clearly demonstrates the interest within academia for this technology.

In recent years, several review articles and critical views on nano- Fe^0 for environmental remediation have been published [20, 24-40]. However, the original discussion on the suitability of nano- Fe^0 for in-situ field applications [25] has not been satisfactorily addressed [28,36]. Moreover, a recent comparison between field applications of Fe^0 of different particle sizes (nm, μm , and mm) for field applications has clearly demonstrated the superiority of mm- Fe^0 (average efficacy 97 %) [11]. The decreasing order of reactivity was mm- Fe^0 (97 %) >

$\mu\text{m-Fe}^0$ (91 %) > nano-Fe^0 (65 %). Expectably, the lower efficiency of nano-Fe^0 is due their high reactivity [25,34]. Therefore, the question arises on the fundamental necessity to further increase the reactivity of nano-Fe^0 by using a noble metal combination.

1.1 The problem

Nano-Fe^0 technology for environmental remediation was introduced as an alternative to the conventional Fe^0 walls mostly for inaccessible aquifers [27,41]. The very small particle size of nano-Fe^0 (1–100 nm) would allow the material to penetrate deep into soil networks [11,12,20,39,40,42].

Due to the exponential relationship between specific surface area (SSA) and radius ($R = d/2$) of a perfectly spherical object ($\text{SSA} = 4\pi R^2$), as a rule, a decrease in Fe^0 particle size increases the surface area per gram by up to 3 orders of magnitude [22,29]. In other words, the inverse relationship between Fe^0 particle size and reactivity is due to a greater density of reactive sites on the particle surface at smaller scale. The following three claims have been made with regard to the use of nano-Fe^0 for aqueous contaminant removal (ref. [12] and ref. therein): (i) some aqueous contaminant species that have been proven as unsuccessful for remediation using $\mu\text{m-Fe}^0$ and mm-Fe^0 can be effectively removed using nano-Fe^0 , (ii) nano-Fe^0 can be used for more rapid degradation of contaminants, and (iii) the formation of some undesirable by-products during remediation using $\mu\text{m-Fe}^0$ and mm-Fe^0 can be avoided by using nano-Fe^0 . Such processes whilst correct are all linked to the greater reactivity nano-Fe^0 possesses due to its size (reactive surface area). When performed in conditions without a large nano-Fe^0 stoichiometric excess, e.g. a system analogous to the environment, it may prove that such claims will be unfounded [21,34,36,43,44].

An undisputed drawback with regards to the use of nano-Fe^0 for environmental applications is their strong tendency to aggregate and adhere to solid surfaces [11,12,20,27,30,39,40,43]. Karn et al. [20] listed some parameters that influence nano-Fe^0 adsorption onto soil and aquifer materials: (i) the surface chemistry of soil and Fe^0 particles, (ii) the groundwater

chemistry (e.g., ionic strength, pH and presence of natural organic matter), and (iii) the hydrodynamic conditions (pore size, porosity, flow velocity and degree of mixing or turbulence). Several methods have been developed for the stabilization of nano-Fe⁰ particles over the past decade and proven efficient to sustain the reactivity of nano-Fe⁰ [11,12,20,43]. One factor that has been overlooked, however, is the impact volumetric expansion has on the mobility of (i) residual Fe⁰, (ii) primary corrosion products (Fe^{II} and H₂) and contaminants. The volume of any corrosion product (Fe hydroxide or oxide) is higher than that of the original metal (Fe⁰). The ratio between the volume of expansive corrosion product and the volume of iron consumed in the corrosion process is called "rust expansion coefficient" (η) [45-47]. Volumetric corrosion products are likely to: (i) contribute to porosity loss, (ii) impact the retention of contaminants and transformation products, and (iii) increase the particle agglomeration.

Another area of heightened research is with regard to the determining the toxicity of nano-Fe⁰, with mixed results reported [12,48]. For example, Barnes et al. [49] reported minimal change to the structure of a river water community due to the addition of nano-Fe⁰, while Diao and Yao [50] reported nano-Fe⁰ particles as highly cytotoxic towards both gram-positive and gram-negative bacteria species.

While taking into account all known influencing parameters, the following seven features have to be systematically studied in order to optimise the general applicability of this technique [12,20,51]: (i) mobility changes due to nano-Fe⁰ volumetric expansion during corrosion, (ii) the bioavailability of Fe⁰ and corrosion products (Fe^{II}/Fe^{III} species, H/H₂), (iii) the ecotoxicity of Fe⁰ and its corrosion products, (iv) the bioaccumulation of Fe⁰ and its corrosion products, (v) the translocation potential of nano-Fe⁰, (vi) the long-term reactivity of nano-Fe⁰ particles, and (vii) the speciation, persistence and fate of contaminants and their transformation products. A major contributing factor to the latter point is that little is known

(compared to permeable reactive barrier technologies) about the extent contaminants are removed via size exclusion using nano-Fe⁰.

Only when all seven “operational drivers” have been determined can the global community have full faith in the technology.

1.2 Objectives of the study

The present communication is focused on the “field persistence” or reactive “life span” of nano-Fe⁰ particles. For in-situ applications a keen understanding of nano-Fe⁰ reactive fate is essential for effective and prudent site clean-up. The knowledge of which is likely to largely underpin decisions as to the (i) the choice of material selected, (ii) the mechanism of application and, (iii) the strategy (if any) for repeated treatments.

In the current work a multidisciplinary approach is used to analyse the relationship between nano-Fe⁰ reactivity and its performance for in-situ field applications. The discussion is based on the contemporary knowledge of the mechanism of aqueous contaminant removal by Fe⁰ [52-54]. Much of the impetus for this work has come from the work of Noubactep and Caré [34], who have challenged the concept that nano-Fe⁰ is a strong reducing agent for contaminant reductive transformation.

2 Nanoscale metallic iron or environmental remediation

To date, nano-Fe⁰ particles have been reported as largely successful for water and soil treatment [11,31,32,55,56]. A wide variety of redox-amenable organic and inorganic species and non-reducible species (e.g. Cd, Zn) have been efficiently treated. Similar to μm and mm -Fe⁰, adsorption is considered important only for non-reducible species [52-54, 57-60]. For example, Boparai et al. [59] reported that heavy metals are either reduced (e.g. Cu²⁺, Ag²⁺) at, or directly adsorbed (e.g. Zn²⁺, Cd²⁺) onto the Fe⁰ surface. They further argued that “the controlling mechanism is a function of the standard redox potential of the contaminant”. Recent work has however challenged this concept [36,54], which is explained below.

2.1 Contaminant reduction by nano-Fe⁰

The chemical reaction between Fe^0 and redox-amenable aqueous species is considered to involve three steps: (i) direct electron transfer from Fe^0 at the metal surface or through a conductive oxide film on Fe^0 (direct reduction), (ii) catalyzed hydrogenolysis by the H/H_2 (indirect reduction mechanism 1), and (iii) reduction by Fe^{II} species resulting from Fe^0 corrosion (indirect reduction mechanism 2). In this constellation, H_2 is supposed to result from H_2O reduction during anoxic iron corrosion [22,61]. However, evidence exists in the literature, e.g. Stratmann and Müller [62], that even under external oxic conditions, Fe^0 is oxidized by H_2O (or more precisely by H^+) and O_2 by Fe^{II} (Table 2). Despite the significant reaction rate exhibited by nano- Fe^0 due to its high surface area, such processes are considered to occur (discounting any quantum size effects) independent of particle size.

Table 2 summarizes the half reactions for the aqueous oxidation of Fe^0 under both anoxic and oxic conditions. Thermodynamically, the major cathodic reaction depends on the availability of molecular O_2 ($E^0 = 0.81 \text{ V}$). In the absence of O_2 , Fe^0 is oxidized by H^+ ($E^0 = 0.00 \text{ V}$). It can therefore be stated that the rate of Fe^0 oxidation is dictated by the concentration of dissolved O_2 , H^+ and H_2O in proximity to Fe^0 surfaces. Le Chatelier's principle also states that the consumption of Fe^{II} (via oxidation to Fe^{III}) will also result in an increase in Fe^0 oxidation. The electrode potential of the redox couple $\text{Fe}^{\text{II}}/\text{Fe}^0$ is -0.44 V , a value which is independent of the particle size (nm, μm or mm). The value -0.44 V is considered largely unchanged due to the presence of alloying materials (e.g. low alloy steel, bimetallic systems).

As a consequence, statements including “*nano- Fe^0 are more reactive than $\mu\text{m-Fe}^0$ and mm- Fe^0* ” are misleading; as the reactivity of Fe^0 (discounting quantum size effects), is independent of the particle size. Any enhanced reactivity reported is likely to be due to the significantly high surface area of nano- Fe^0 compared to other forms. A second statement “*bimetallic nano- Fe^0 is more reactive than monometallic nano- Fe^0* ” is also a qualitative statement, as the reactivity of the materials depends on numerous factors associated with the materials synthesis route and varies depending on the chemistry of the chosen alloying metal. Ideally,

comparisons should be made versus standard reference materials using established standard experimental protocols [63], which once established, will significantly improve the design of future field applications.

2.2 Limitations of the nano-Fe⁰ technology

The efficiency of nano-Fe⁰ for aqueous contaminant reduction faces some key issues for in-situ applications in porous media. These challenges include: (i) the strong tendency of aggregation/agglomeration, (ii) the rapid settlement on subsurface solid phases, (iii) the porosity and permeability loss of porous media [23,35,64,65]. Aggregation and settlement limit nano-Fe⁰ transport through porous media. Porosity and permeability loss limit nano-Fe⁰ transport to target contaminants. It was demonstrated that nano-Fe⁰ may travel only a few centimetres in porous media from the injection position under typical groundwater conditions [11,12,30,66]. Accordingly, recent efforts have been made to (i) increase the porosity of porous media, (ii) mechanically increase the distribution of nano-Fe⁰, and/or (iii) chemically modify nano-Fe⁰ for improved aqueous mobility in porous networks.

2.3 Improving the efficiency of the nano-Fe⁰ systems

2.3.1 Dispersion agents

Methods to improve the aqueous mobility of nano-Fe⁰ have received the greatest research interest. It has been determined that the key to improving particle mobility is found in modifying their surface properties such that the nano-Fe⁰ have significantly improved colloidal stability and a commensurate reduction in the likelihood of adherence to mineral surfaces. Several synthetic methods are now available to produce more mobile nano-Fe⁰. Efficiently tested dispersants include anionic surface chargers (e.g. polyacrylic acid), non-ionic surfactants, starch, and oil [23,67-70].

2.3.2 Bimetallic combinations

In recent years, noble metals have been used to increase the reactivity of monometallic nano-Fe⁰ [21,23,71-73]. As mentioned above, this appears counterintuitive as nano-Fe⁰ is already

high reactivity due to its size [15,26,29,42] and is unstable during synthesis, storage and application [69]. This chemical instability has been documented as a key reason for the observed lower efficiency exhibited by nano-Fe⁰ systems compared to μm and mm-Fe⁰ [11]. Accordingly, it is questionable whether further enhancing the reactivity of nano-Fe⁰, e.g. by plating with more noble elements, may be of any benefit. The reactivity of nano-Fe⁰ will be discussed in the next section on the basis of mathematical modelling.

3 Significance of increased reactivity

3.1 The problem

The increased Fe⁰ reactivity from mm to nm size should be better characterized. The relative reactivity of four different materials is discussed on the basis of 1 kg Fe⁰: one nm-Fe⁰ (d₀ = 25 nm), one μm-Fe⁰ (d₀ = 25 μm), and two mm-Fe⁰ (d₀ = 250 and 1000 μm). Calculations for the number particles (N) in 1 kg of each material and the number of layers (N') in each particle are made after the Eq. (1) and Eq. (2) presented in details elsewhere [9,74].

$$N = \frac{M}{\rho_{\text{Fe}} \cdot 4/3\pi \cdot R_0^3} \quad (1)$$

$$N' = 2 \cdot [4/3(\pi R_0^3)]/a^3 \quad (2)$$

where M is the mass of Fe⁰ (here 1 kg), ρ_{Fe} is the specific weight of Fe (7,800 kg/m³), R₀ is the initial radius of the Fe particle (d = 2·R₀) and a the lattice parameter (a = 2.866 Å).

The results are summarized in Table 3. It can be seen that the number of layers of Fe⁰ in individual particles varies from 87.2 for nano-Fe⁰ to more than 3·10⁶ for mm-Fe⁰ (d = 1 mm). In the meantime, the number of particles in 1 kg decreased from 1.96·10¹⁸ for nano-Fe⁰ to only 3.1·10⁴ for mm-Fe⁰. The ratio of the number of Fe⁰ layers in each particle to the number of Fe⁰ layers in nano-Fe⁰ varies from 1 to 4·10⁴. This ratio corresponds to the relative time (τ) as defined later (section 3.2). On the other hand, the ratio of the number of particles in 1 kg of nano-Fe⁰ to the number of particles in the same mass of each other materials varies from 1 to

6.4*10¹³. These results are summarized in Fig. 1. Instead of the mass of Fe⁰, the number of electrons released by the conversion of Fe⁰ to Fe^{II} is used to assess the kinetics of Fe⁰ consumption. This is discussed in the next section.

3.2 Relative corrosion kinetics of Fe⁰ materials

For the discussion in this section, uniform corrosion for spherical particles is assumed. Individual particles corrode independently until material depletion. It is further assumed for simplicity that individual layers corrode with the same kinetics independent of particle size ($d = 2 \cdot R_0$). The latter assumption is conservative as larger particles react slower than smaller [24,29,61]. With these assumptions, a relative time (τ) can be defined while taking the time for the corrosion of the smallest particle (here 87.2 layers of nano-Fe⁰) or $t_{\infty, \text{nano}}$ as unit.

$$\tau = t/t_{\infty, \text{nano}} \quad (3)$$

Accordingly, one unit of time corresponds to the time to nano-Fe⁰ depletion. Remember that all 1.96*10¹⁸ particles in the 1 kg of nano-Fe⁰ simultaneously corrode with the same kinetics. The results of the calculations are presented in Fig. 2. From Fig. 2a and Tab. 3 it can be seen that after nano-Fe⁰ depletion, the material with 1000 μm (or 1 mm) diameter will still react for more than 3*10⁴ times longer than the time necessary for nano-Fe⁰ depletion ($\tau = 4 \cdot 10^4$, see Tab. 3). Fig. 2b shows that the mm-Fe⁰ with 250 μm diameter is depleted after about 10⁴* $t_{\infty, \text{nano}}$.

Based on the assumptions above, the service life of a nano-Fe⁰ particle can be estimated. Table 4 summarizes the results of such estimations while varying the service life of a 1 mm Fe⁰ particle from 5 to 40 years. This assumption is based on the fact that conventional Fe⁰ walls are supposed to function for several decades (here up to 4 decades). Results show (Tab. 4) that the maximum life-span of a nano-Fe⁰ is about 8.8 hours (less than one day). In other words, following approximately 9 hours from subsurface deployment it is suggested that all nano-Fe⁰ would be reactively exhausted. The success of this is dependent on three key

factors: (i) the hydrodynamic conditions: pore size, porosity, flow velocity and degree of mixing or turbulence, (ii) the water chemistry and the affinity of nano-Fe⁰ and its transformation products to the soil materials, and (iii) the reactivity of Fe⁰.

It is certain, that the dynamic process of transformation of concentric layers of Fe⁰ atoms to concentric layers of iron (hydr)oxides can not be linear [34]. In fact, effects similar to "case hardening" for food- and wood-drying will lead to "surface hardened layers" [75, 76] leading to differential kinetics/extents of Fe⁰ passivation for different particle size ranges. In other words, the extend of restricted corrosion rates through resulting surface hardened layers will be different for nm-, µm- and mm-Fe⁰. Bearing this in mind, the very short relative life-span of a nano-Fe⁰ estimated above will be used for the discussion in this work. It is certain that "case hardening"-like effects will prolong this hypothetical life-span to some days or weeks.

3.3 Extent of iron corrosion from Fe⁰ materials

A discussion as to the extent of Fe⁰ consumption is limited in the present section to $\tau = 1$ or $t_{\infty, \text{nano}}$. It is considered for simplification that the sole iron corrosion product is Fe₃O₄. The corresponding coefficient of volumetric expansion is $\eta_{\text{Fe}_3\text{O}_4} = 2.08$ (Eq. 4) [46]. Using $\rho = M/V$, the volume of Fe corresponding to 1 kg Fe⁰ is calculated as 127.0 mL (V_0). This is the initial volume of Fe⁰ (V_0). Following corrosion, this volume is partly or totally consumed. The volume (ΔV) corresponding to the volume of pores occupied by the volumetric expansion of corrosion products can be estimated.

Assuming that the coefficient of volumetric expansion (η) ("rust expansion coefficient" or "specific volume") [45-47] of the reaction products is:

$$\eta = V_{\text{oxide}}/V_{\text{Fe}} \quad (4)$$

where V_{oxide} is the volume of the reaction product and V_{Fe} the volume of the parent Fe⁰.

The volume ΔV characterizing the extent of porosity loss due to volumetric expansion is given by Eq. 5:

$$\Delta V = (\eta - 1) * V_{\text{consumed Fe}} \quad (5)$$

$$\Delta V = V_{\infty} - V_0 = v * (\eta_{\text{Fe}_3\text{O}_4} - 1) * V_0 \quad (5a)$$

Where $V_{\text{consumed Fe}}$ is the volume of consumed Fe^0 at time t_{∞} , V_0 is the volume occupied by the initial Fe^0 particles and v ($v \leq 1$) is the fraction of the initial amount of Fe^0 (1 kg) which has reacted at $t_{\infty, \text{nano}}$. V_{∞} is the total volume occupied by residual Fe^0 and in-situ formed corrosion products. t_{∞} corresponds to nano- Fe^0 depletion (25 nm in this section). In the discussion on the reactivity at nano-scale, t_{∞} corresponds to the depletion of the material with 10 nm diameter (section 4).

$$V_{\infty} = \eta * V_{\text{consumed Fe}} + (V_0 - V_{\text{consumed Fe}}) \quad (6)$$

$$V_{\infty} = V_0 [1 + v * (\eta_{\text{Fe}_3\text{O}_4} - 1)] \quad (6a)$$

The volumetric expansion (ΔV , Eq. 5) can be characterized as percent of the initial volume (V_0) using Eq. (7):

$$\Delta V (\%) = 100 * v * (\eta_{\text{Fe}_3\text{O}_4} - 1) \quad (7)$$

Table 5 summarizes the results. It is shown that at $\tau = 1$ (nano- Fe^0 depletion), a volume augmentation of 108 % has occurred in the nano- Fe^0 system, with volume augmentations in all other systems lower than 0.5 %. This clearly shows that the porosity of the subsurface will be significantly influenced by nano- Fe^0 at t_{∞} . Remember that 100 % reactive exhaustion of nano- Fe^0 is predicted to occur by approximately 9 hours time. During this same period the porosity loss due to expansive iron corrosion is likely to be negligible for all other Fe^0 particle size fractions. Calculations for Akageneite $\beta\text{-FeOOH}$ ($\eta_{\text{FeOOH}} = 3.48$) as sole corrosion products shows that $V_{\infty, \text{nano}} = 448.7$ mL, $\Delta V = 320.5$ mL or 250.4 %. The examples of Fe_3O_4 (anoxic) and FeOOH (oxic) demonstrate the crucial importance of the nature of formed corrosion products for the discussion of the extent of porosity loss.

Another important aspect of Fe^0 consumption is given by the number of moles of Fe^0 that have been oxidized (Tab. 5). Assuming contaminant reduction, Tab. 5 shows that after $\tau = 1$,

35.71 moles of electrons have been released in the nano-Fe⁰ system but less than 0.11 moles in all other systems. In other words, up to 35.71 moles of electrons are available for contaminant reduction per kg nano-Fe⁰ within a few hours of reaction (< 9 hours). But what proportion of the electrons produced would reach the contaminant within this period? That is the major question to be answered for the further development of the nano-Fe⁰ technology for in-situ applications.

4 Reactivity of nano-Fe⁰ materials

The presentation until now has discussed the reactivity of nano-Fe⁰ in comparison to larger scale Fe⁰. Section 4 will focus only on the nanoscale size fraction ($d \leq 100$ nm). Equations 1-7 will be used and the particle size will vary from 10 to 100 nm. As stated above t_{∞} is for a nano-Fe⁰ of 10 nm diameter and the reaction proceeding until 100 % reactive exhaustion has been achieved.

4.1 Fe⁰ reactivity at nanoscale

Table 6 summarizes the results of calculations for the number of Fe⁰ particles and number of layers of Fe⁰ in each nano-Fe⁰. It is shown that 1 kg of the material with $d = 100$ nm contains 1000 times more particles than a material of $d = 10$ nm.

Table 6 also shows that the maximum value of the relative time (τ) is 10 (or 10^1). This is more practical for graphical representations than situations where nano-Fe⁰ are compared to larger particles ($t \leq 10^4$). The physical significance of τ is more important, it means that if a nano-Fe⁰ with a diameter of 10 nm depletes after 2 days, the material with a diameter 100 nm will deplete after 20 days. For field applications the selection of the particle size to be used should be dictated by site specific characteristics. Which diameter could quantitatively reach the contaminants before depletion? And what fraction of the material will have already oxidized on the path? What is the impact of this oxidation on the transport of nano-Fe⁰ in the porous aquifer? These are some key questions to be answered in order to give this possibly very efficient technology a scientific basis.

Fig. 3 summarizes the evolution of the volumetric expansion in all 5 nano-Fe⁰ systems. It can be seen from Fig. 3a that the smallest material (d = 10 nm) experiences the 108 % volumetric expansion within a short time ($\tau = 1$) while the larger materials (d = 100 nm) needs 10 more time for the same expansion. Accordingly, beside the question whether the material will reach the contaminant under site specific conditions, the question has to be answered how the volumetric expansion will impact the aquifer porosity (and permeability).

Fig. 3b compares the variation of the volumetric expansion for two different iron corrosion products, Fe₃O₄ and FeOOH, which are considered the most likely products in anoxic and oxic aquifers respectively. It also shows that when designing a nano-Fe⁰ injection strategy, however, the availability of oxidizing species (e.g. MnO₂, O₂) must also to be taken into account. Fig. 3a shows that under both conditions the trend of porosity loss is similar but the extent is proportional to the coefficient of volumetric expansion (η). In particular, at $\tau = 1$, the system with the material d = 10 nm experiences 250 % volumetric expansion under oxic conditions and only 110 % under anoxic conditions. As a result the kinetics of more rapid Fe⁰ corrosion in an oxygen-rich environment must also be considered for an effective treatment strategy.

4.2 Fe⁰ reactivity of nano-bimetallics

The reactivity of monometallic nano-Fe⁰ can be improved by combining it with a noble metal. Assuming α ($\alpha > 1$) the coefficient of reactivity enhancement, the relation between the relative time of a bimetallic system ($\tau_{Fe/M}$) and that of a non plated metal (τ_{Fe}) is given by Eq. 6:

$$\tau_{Fe} = \alpha * \tau_{Fe/M} \quad (8)$$

To characterize the impact of plating on nano-Fe⁰, the material with the largest size (d = 100 nm) will be plated by three hypothetical metals (M⁰₁, M⁰₂ and M⁰₃) to yield a reactivity factor of 2.5 (for Fe⁰/M⁰₁), 5 (for Fe⁰/M⁰₂) and 10 (for Fe⁰/M⁰₃). The considered α values of ($\alpha \leq 10$)

are realistic and even conservative. In fact, reported reactivity enhancement is essentially larger [22,77]. For example, Zhuang et al. [77] reported that palladized nano-Fe⁰ promoted the dehalogenation kinetics for polybrominated diphenyl ethers by orders of magnitude equal to 2, 3 and 4 ($\alpha \geq 100$). The results of the calculations for the four systems ($d = 10$ nm) are summarized in Fig. 4. The system with $d = 10$ nm is represented for comparison. It can be seen that system Fe⁰/M₃⁰ ($d = 100$ nm) is as reactive as Fe⁰ ($d = 10$ nm). Given that the reactivity of nano-Fe⁰ ($d = 100$ nm) could already significantly been too high in some situations, the results from Fig. 4 strongly question the suitability of plating at nano-scale. Accordingly, while the application of bimetallic Fe⁰ is definitively useful at μ m- and mm-scale, its usefulness at nano-scale is likely inappropriate. It can also be noted that by increasing the reactivity of the material the rate at which volumetric pore clogging also increases. As a consequence it should be acknowledged that there exists a conceptual play-off between increased reaction rate and increased porosity loss, the impact of which will vary depending on the physiochemical conditions of each contaminated site.

4.3 Characterizing the process of reactivity loss

To better characterize the process of porosity loss due to the volumetric expansion of nano-Fe⁰, the evolution of the porosity of a sand column filled with nano-Fe⁰ will be discussed as volumetric expansion proceeds. A laboratory column with a height h ($h = 75.0$ cm) and diameter D ($D = 5.0$ cm) is composed of spherical sand particles ($d = 5.0$ mm). The compactness of the column is ideally $C = 0.64$ [9,74]. The pore volume is given by Eq. 9:

$$V_{\text{pore}} = V * (1 - C) \quad (9)$$

where V is the apparent volume of the sand column ($V = h * \pi * D^2/4$).

It is supposed that the nano-Fe⁰ particles fill the inter-granular porosity of the sand column V_{pore} without modifying the compactness C and the apparent volume V of the sand column. The residual porosity of the sand column (V'_{pore}) is given by Eq. 10:

$$V'_{\text{pore}} = V*(1-C) - V_0 \quad (10)$$

where V_0 is the volume of the Fe particles.

The evolution of the residual porosity (V'_{pore}) as nano-Fe⁰ particles undergo volumetric expansive corrosion is considered by introducing the specific volume (η) of the reaction products according to Eq. 11:

$$V'_{\text{pore}} = V(1 - C) - (V_0 - V_{\text{consumed Fe}}) - \eta * V_{\text{consumed Fe}} \quad (11)$$

$$V'_{\text{pore}} = V(1 - C) - V_0 - (\eta - 1) * V_{\text{consumed Fe}} \quad (11a)$$

where $V_{\text{consumed Fe}}$ is the volume of nano-Fe⁰ particles which is consumed at a given time.

Equations 9 through 11 are very useful to design reactive zone. However, they are limited to describe the initial (V_{pore}) and a final conditions (V'_{pore}) regardless on the nature of iron corrosion products and the kinetics of the process.

Using a sand column comparable to one of those used by Moraci and Calabrò [78] and 1 kg of nano-Fe⁰, the process of pore filling (porosity loss) can be better characterized. For simplicity nano-Fe⁰ considered as transported by a biodegradable dispersant which does not significantly contribute to porosity loss. As shown in section 3.3, 1 kg of nano-Fe⁰ occupies a volume of 127 mL. The initial pore volume of the sand column calculated after Eq. 9 is 530.36 mL (100 % porosity), i.e. a capacity for approximately 4.17 kg of nano-Fe⁰. Filling the initial pore volume of the sand column (530.36 mL) with 1 kg of nano-Fe⁰ (127.00 mL) yields a 23.9 % porosity loss (Tab. 7). This, however, does not take into account the expansive nature of iron during oxidative corrosion.

Using the 8 possible iron corrosion products documented by Caré et al. [46] and their respective coefficient of volumetric expansion ($2.08 \leq \eta \leq 6.40$), the extent of porosity loss is calculated and summarized in Table 7. The results show that the residual volume of pores (V'_{pore}) decreases with increasing η values and is zero for Fe(OH)₃ and Fe(OH)₃.3H₂O (100 % porosity loss). Ferrihydrite (Fe(OH)₃.3H₂O) is the largest known iron corrosion products. In other words, depending on environmental conditions as little as 1 kg of nano-Fe⁰ could clog the tested column. Although this discussion considers the nature of the corrosion

products, there are other important factors which must be considered. The negative values (-3.04 and -282.4 mL) corresponds to the mass of Fe^0 which will not oxidized because of lack of space for expansion [9,74].

The extent of porosity loss (ΔV in %) given in Tab. 7 assumes uniform distribution of nano- Fe^0 in the whole column. This is, however, not a very good field representation. For example, if 1 kg of nano- Fe^0 ($V_0 = 127$ mL) is uniformly distributed only in the first third of the column ($V_{\text{pore}}^{1/3} = 176.8$ mL), with Fe_3O_4 as the primary corrosion product ($\Delta V = 137.16$ mL) a 78 % porosity loss can be expected. For all other oxide phases it is calculated that complete porosity loss (100 %) will precede nano- Fe^0 reactive exhaustion. However, in the practice a system with 78 % porosity loss is considered as clogged. One possibility to avoid the clogging of the entrance zone of a porous system is to intermittently inject calculated amounts of nano- Fe^0 . The volume to be injected at each event and the time scale between two injections are necessarily determined by site specific characteristics (e.g. aquifer porosity, water flow rate).

5 Discussion

A primary reason behind the interest into the use of nano- Fe^0 particles over $\mu\text{m-Fe}^0$ and mm- Fe^0 particles for water treatment is ascribed to a significant increase the materials efficiency [11,12]. For example, as reported by Vodyanitskii [79], Kanel et al. [80] reported near-total remediation of a $1 \text{ mg L}^{-1} \text{ As}^{\text{V}}$ solution within only 10 min by a nano- Fe^0 with a specific surface of $24 \text{ m}^2/\text{g}$, whereas the same goal was achieved by mm- Fe^0 ($1\text{--}2 \text{ m}^2/\text{g}$) after only 4 days or 5760 min (ratio of time 570; average ratio of surface 16). However, this experimental evidence is highly qualitative as neither the number of atoms directly accessible at the surface nor the intrinsic reactivity of individual materials are considered in both cases [34]. For a better comparative result, the following three key conditions must be considered: (i) the intrinsic Fe^0 reactivity should be characterized, (ii) the amount of used materials should be based on the reaction stoichiometry, and (iii) the experimental conditions should be relevant for field applications. In particular, the driving force for the transport of contaminants and Fe

species should be relevant for field situations: (i) mixing operation (type and intensity) in batch studies, (ii) flow rate and column dimensions in column studies [63].

5.1 Transport of nano-Fe⁰ to the contaminants

The efficiency of nano-Fe⁰ for the in-situ treatment of a contaminated aquifer body is intrinsically linked to the extent of physical contact between Fe⁰ and any aqueous contaminant species present. In some circumstances, contaminants could diffuse to the suspended Fe⁰ particles and be degraded in the aqueous phase. However, typically the suspended Fe⁰ particles must migrate to the contaminants. As Fe⁰ particles are transported from the injection zone to the target contaminant plume by natural groundwater, diffusion experiments under relevant groundwater velocity, using site specific aquifer materials are essential in order to effectively assess the suitability of nano-Fe⁰ for in-situ applications [81].

Contaminants are typically partitioned between sediment and water phases in a “pseudo-equilibrium” state. Therefore, it is likely that Fe⁰ particles whilst acting to reduce any soluble contaminants are also likely to promote the dissolution of a range of adsorbed chemical species (Le Chatelier’s principle). However, as water is also a redox-amenable species the specific mechanism for nano-Fe⁰ reactivity in a range of conditions is difficult to resolve [30]. In other words, nano-Fe⁰ is readily oxidized by H₂O during subsurface migration to the target contaminant plume and also competes with any other redox-amenable (including contaminants) present in the groundwater. Additionally, expansive iron corrosion will yield voluminous iron (hydr)oxides (Tab. 7) with limited aqueous mobility due to (i) an increased size and weight, and (ii) a possible increased affinity to aquifer material.

This discussion has intentionally neglected the segregation between parent compounds, the reaction products and their relative affinity to Fe⁰ and Fe (hydro)oxides. The fact that the core Fe⁰ is always covered by oxide layers is also neglected for simplification. The process of preferential flow which is crucial in predicting mass transfer in the subsurface is also not considered [82-84]. However, it is clearly shown, that due the acute redox sensitivity of nano-

Fe⁰ and the subsequent significant formation of highly voluminous oxidative corrosion products it is likely that for environmentally relevant distances (m), a significant proportion of the originally injected nano-Fe⁰ will remain “clogged” in pore spaces.

Beside the transport of nano-Fe⁰ to contaminants, the possibility of quantitative contaminant desorption and their subsequent transformation by suspended Fe⁰ could be considered. However, it is not likely that concentration-gradient-driven mass transfer could be quantitative at considered distances (m). It should be recalled that the slow kinetics of contaminant desorption from aquifer materials is the major cause of the ineffectiveness of the pump-and-treat technology for groundwater remediation [87-89].

This section has shown that it is likely that the success of nano-Fe⁰ for in-situ remediation is seriously limited by the intrinsic formation of voluminous iron corrosion products [11,12,30,39,40]. Bearing this in mind, the next section suggests an alternative nano-Fe⁰ subsurface deployment mechanism that more effectively takes into account the aforementioned nano-Fe⁰ hydraulic mobility issues than conventional injection processes: the formation of a nano-Fe⁰ “redox-front” injection array system for progressive contaminant reduction. The geochemical process of redox-front migration is a well-documented one [83,90,91].

5.2 Nano-Fe⁰ as source of Fe^{II} for a redox-front?

5.2.1 The concept

The progressive consumption of mm-Fe⁰ (Fig. 1; Tab. 3) is the guarantee for the long-term efficiency of reactive barriers [11]. In fact, continuously generated small amount of high reactive iron minerals [36,52-54,92-95] are sufficient for the removal of contaminants which are present in trace amounts [96]. As discussed above, for nano-Fe⁰ however, (i) Fe⁰ reactive exhaustion typically occurs in a relatively short time scale (< 9 hours) and, (ii) it is likely that nano-Fe⁰ subsurface mobility is significantly retarded or even prevented due to the volumetric expansive nature of iron corrosion [46]. As a consequence an alternative method of

subsurface deployment is suggested in the current work: the deployment of a linear nano-Fe⁰ injection array orientated perpendicular to the flow direction of the contaminant plume. The injected nano-Fe⁰ can effectively form a redox-front (roll-front) which migrates through the contaminated zone and transforms the contaminants during its migration as illustrated in Fig. 5. The Fe^{II}/Fe^{III} roll-front travels across the contaminated zone with all possible mechanisms (e.g. diffusion, dispersion, convection, preferential flow) and the contaminants are transformed and immobilized during the cycle Fe^{II} ⇌ Fe^{III}. In other words, it is a plume of Fe^{II}/Fe^{III} formed from injected nano-Fe⁰ which migrates through the contaminated zone and “sweeps” the contaminants. As a consequence this method considers all nano-Fe⁰ mobility issues.

5.2.2 Nano-Fe⁰ as Fe^{II} generator

Nano-Fe⁰ in the aqueous phase is certainly a Fe^{II}/Fe^{III} producer. Fe^{II}-species are the main reducing agents for contaminants under both anoxic and oxic conditions [62]. The reducing capacity of Fe^{II}-species nominally depends on the pH value [54,77,97,98]. Microbial activity could regenerate Fe^{II} (bio-corrosion) for more contaminant reduction [79]. In this case, more contaminant is reduced than can be predicted from the reaction stoichiometry. In other words, the operating mode of nano-Fe⁰ for contaminant reduction can be summarized as follows: (i) Fe⁰ is oxidized to produce Fe^{II}, (ii) Fe^{II} reduces the contaminant and is oxidized to Fe^{III}, and (iii) a proportion of Fe^{II} is regenerated by the biological reduction of Fe^{III}. Accordingly, before Fe⁰ depletion, there are three sources of Fe^{II}: (i) the Fe⁰ mediated abiotic oxidation by H₂O, (ii) the Fe⁰ mediated abiotic oxidation by Fe^{III}, and (iii) the biological reduction of Fe^{III}. After Fe⁰ depletion, the only remaining source of Fe^{II} is the biological reduction of Fe^{III}. Provided that the appropriate micro-organism species are present in the subsurface, this process, however, could conceptually proceed for a significantly long time period [35]. Evidence suggests that such micro-organism colonies can be sustained by a consistent supply of Fe^{II}, Fe^{III} and molecular hydrogen (H₂). Another further process that is worth noting is

the generation of atomic or molecular hydrogen (H/H_2) by Fe^0 mediated hydrolysis reactions, which is likely to aid and the aforementioned biotic processes [35].

The abiotic conversion of Fe^{III} to Fe^{II} has been successfully utilised in the hydrometallurgy industry, for example Lottering et al. [99] reported on the sustainable use of MnO_2 for the abiotic regeneration of Fe^{III} for U^{IV} oxidation.

The fate of contaminant reduction products is discussed in the next section.

5.3 Mechanism of contaminant removal by injected nano- Fe^0

The successful application of nano- Fe^0 injection technology for in-situ remediation is highly dependent on a comprehensive understanding of the fundamental processes governing the processes of contaminant removal. The hitherto discussion has focused on reductive transformations by nano- Fe^0 . However, contaminant reductive transformation is not a guarantee for contaminant removal [52-54]. Additionally, certain reaction products are more toxic than their parent compounds [100]. Accordingly, efforts have to be focused on the specific mechanism of aqueous contaminant removal. Relevant removal processes include: (i) adsorption, (ii) chemical precipitation, (iii) co-precipitation, (iv) size exclusion or straining, and (v) volatilization [52-54,79,101-104]. Chemical precipitation is a characteristic of inorganic compounds when the solubility limit is exceeded [101,102,105]. Volatilization is subsequent to chemical transformation yielding gaseous species like AsH_3 , CH_4 , CO_2 , H_2 , N_2 . In Fe^0 reactive barrier systems, contaminants are efficiently removed by the combination of adsorption, co-precipitation and size exclusion within the engineered barrier [14,106]. As a result the current discussion concentrates on such processes..

With Fe^0 ($< 1\text{ m}^2/\text{g}$) first transformed to voluminous hydroxides species ($> 100\text{ m}^2/\text{g}$) and subsequently transformed to oxides ($< 40\text{ m}^2/\text{g}$), contaminant size exclusion (straining) is driven by the dynamic cycle of expansion/compression accompanying the corrosion process [14,107]. During these cycles contaminants are enmeshed and sequestered in a “matrix” of iron corrosion products.

For conventional nano-Fe⁰ injection arrays, size exclusion may play an important role (i) in proximity for Fe⁰ particles, and (ii) by reducing the pore space during expansive corrosion of the materials. However, if roll-fronts are formed as discussed above, the extent of permeability loss in aquifer will be limited. The roll-front could act as a colloidal reactive barrier for the removal of parent contaminants and reaction products. Species are removed or immobilized by colloids and not because they are reduced. More research is needed to test this hypothesis.

5.3.1 Fe^{II}/Fe^{III} redox-front as a colloidal reactive barrier

Aqueous contaminants have been reported to be quantitatively removed both during abiotic and biotic (i) oxidation of Fe^{II} and (ii) reduction of Fe^{III} [107-109]. On the other hand, injection of Fe^{III} salts for adsorptive contaminant removal has been reported [110,111]. Accordingly, the migration of the Fe^{II}/Fe^{III}-redox-front may be coupled to quantitative contaminant removal by adsorption and co-precipitation.

The primary reason for contaminant removal during these redox reactions is the colloidal nature of in-situ generated Fe species [Fe(OH)₂, Fe(OH)₃] [112], which necessarily experience volumetric contraction to form oxides (of Fe^{II} or Fe^{III}). Contaminants are first adsorbed by highly reactive colloids and are co-precipitated during transformation to amorphous and crystalline oxides [79,113]

6 Concluding remarks

Constructed geochemical barriers of metallic iron (Fe⁰) have been used for groundwater remediation since 1996 [1,5,6,79,114]. In recent years, however, nano-Fe⁰ has received proclaim as a new tool for water treatment due to (i) improvements in reactivity and associated aqueous contaminant removal performance compared to conventional materials, and (ii) the option of subsurface deployment via injection for targeted in-situ treatment of contaminant plumes [11,12].

541 Considering reactivity first, the current work has highlighted the need for prudent use of
542 terminology. Discounting any quantum size effects, which are only prevalent for Fe^0 less than
543 approximately 10 nm in diameter, the reactivity of nano- Fe^0 as a function of surface area is no
544 more reactive than larger forms. Nano- Fe^0 only exhibits such high reactivity due to its
545 significantly high surface area as a function of mass/volume. Despite this, a recent trend in
546 research has been the development of bimetallic nano- Fe^0 wherein the combination of a noble
547 metal acts to further increase the reactivity of nano- Fe^0 . It is argued in the current work that as
548 reactive exhaustion is already achieved by monometallic nano- Fe^0 in the order of minutes this
549 seems counterintuitive for the majority of environmental applications.

550 Considering the nano- Fe^0 subsurface injection procedure, in the current work it has been
551 highlighted that the hydraulic mobility of the particles is likely to be significantly retarded by
552 voluminous expansion due to particle corrosion. An alternative nano- Fe^0 injection procedure
553 has been suggested herein. The injected nano- Fe^0 effectively forms an in-situ migrating front
554 which possibly reductively transforms contaminant and removes reduced species by
555 adsorption and co-precipitation.

556 It is also outlined in the current work that a number of studies with experiments "proclaimed"
557 as analogous to environmental systems are largely overlooked a range of operational drivers
558 including changes in nano- Fe^0 (i) reactivity, and (ii) voluminous as a function of time. It is
559 hoped that the huge literature on redox-front migration [115-118] and the cycle of iron in the
560 hydrosphere ([79] and ref. therein) will now be used for the further development of nano- Fe^0
561 injection technology.

562 **Acknowledgments**

Mohammad A. Rahman (Angewandte Geologie - Universität Göttingen) is acknowledged for technical support.

Cited References

- [1] R.W. Gillham, S.F O'Hannesin, Enhanced degradation of halogenated aliphatics by zero-valent iron, *Ground Water* 32 (1994) 958–967.
- [2] L.J. Matheson, P.G. Tratnyek, Reductive dehalogenation of chlorinated methanes by iron metal, *Environ. Sci. Technol.* 28 (1994) 2045–2053.
- [3] D.W. Blowes, C.J. Ptacek, J.L. Jambor, In-situ remediation of Cr(VI)-contaminated groundwater using permeable reactive walls: laboratory studies, *Environ. Sci. Technol.* 31 (1997) 3348–3357.
- [4] S.F. O'Hannesin, R.W. Gillham, Long-term performance of an in situ "iron wall" for remediation of VOCs, *Ground Water* 36 (1998) 164–170.
- [5] M.M. Scherer, S. Richter, R.L. Valentine, P.J.J. Alvarez, Chemistry and microbiology of permeable reactive barriers for in situ groundwater clean up, *Rev. Environ. Sci. Technol.* 30 (2000) 363–411.
- [6] A.D. Henderson, A.H. Demond, Long-term performance of zero-valent iron permeable reactive barriers: a critical review, *Environ. Eng. Sci.* 24 (2007) 401–423.
- [7] G. Bartzas, K. Komnitsas, Solid phase studies and geochemical modelling of low-cost permeable reactive barriers, *J. Hazard. Mater.* 183 (2010) 301–308.
- [8] Li L., Benson C.H., Evaluation of five strategies to limit the impact of fouling in permeable reactive barriers, *J. Hazard. Mater.* 181 (2010) 170–180.
- [9] C. Noubactep, S. Caré, Dimensioning metallic iron beds for efficient contaminant removal, *Chem. Eng. J.* 163 (2010) 454–460.
- [10] J.Y. Kim, H.-J. Park, C. Lee, K.L. Nelson, D.L. Sedlak, J. Yoon, Inactivation of *Escherichia coli* by nanoparticulate zerovalent iron and ferrous ion, *Appl. Environ. Microbiol.* 76 (2010) 7668–7670.

- 589 [11] S. Comba, A. Di Molfetta, R. Sethi, A comparison between field applications of nano-,
590 micro-, and millimetric zero-valent iron for the remediation of contaminated aquifers,
591 Water Air Soil Pollut. 215 (2011) 595–607.
- 592 [12] M. Gheju, Hexavalent chromium reduction with zero-valent iron (ZVI) in aquatic
593 systems, Water Air Soil Pollut. (2011) doi 10.1007/s11270-011-0812-y.
- 594 [13] S.-W. Jeon, R.B. Gillham, A. Przepiora, Predictions of long-term performance of
595 granular iron permeable reactive barriers: Field-scale evaluation, J. Contam. Hydrol.
596 123 (2011) 50–64.
- 597 [14] C. Noubactep, Metallic iron for safe drinking water production, Freiberg Online
598 Geology, 27 (2011) 38 pp, ISSN 1434-7512. (www.geo.tu-freiberg.de/fog)
- 599 [15] C.-B. Wang, W.-x. Zhang, Synthesizing nanoscale iron particles for rapid and complete
600 dechlorination of TCE and PCBs, Environ. Sci. Technol. 31 (1997) 2154–2156.
- 601 [16] S.M. Ponder, J.G. Darab, T.E. Mallouk, Remediation of Cr(VI) and Pb(II) aqueous
602 solutions using supported, nanoscale zero-valent iron, Environ. Sci. Technol. 34 (2000)
603 2564–2569.
- 604 [17] R. Muftikian, Q. Fernando, N. Korte, A method for the rapid dechlorination of low
605 molecular weight chlorinated hydrocarbons in water, Water Res. 29 (1995) 2434–2439.
- 606 [18] N.E. Korte, J.L. Zutman, R.M. Schlosser, L. Liang, B. Gu, Q. Fernando, Field
607 application of palladized iron for the dechlorination of trichloroethene, Waste Manage.
608 20 (2000) 687–694.
- 609 [19] B. Schrick, J.L. Blough, A.D. Jones, T.E. Mallouk, Hydrodechlorination of
610 trichloroethylene to hydrocarbons using bimetallic nickel–iron nanoparticles. Chem.
611 Mater. 14 (2002) 5140–5147.
- 612 [20] B. Karn, T. Kuiken, M. Otto, Nanotechnology and in situ remediation: A review of the
613 benefits and potential risks. Environ. Health Perspectives 117 (2009) 1832–1831.

- 614 [21] V. Nagpal, A.D. Bokare, R.C. Chikate, C.V. Rode, K.M. Paknikar, Reductive
615 dechlorination of γ -hexachlorocyclohexane using Fe–Pd bimetallic nanoparticles, J.
616 Hazard. Mater. 175 (2010) 680–687.
- 617 [22] K.-F. Chen, S. Li, W.-x. Zhang, Renewable hydrogen generation by bimetallic zerovalent
618 iron nanoparticles, Chem. Eng. J. (2011), doi:10.1016/j.cej.2010.12.019.
- 619 [23] S. Mossa Hosseini, B. Ataie-Ashtiani, M. Kholghi, Nitrate reduction by nano-Fe/Cu
620 particles in packed column, Desalination (2011) doi:10.1016/j.desal.2011.03.051.
- 621 [24] W.-X. Zhang, C.-B. Wang, H.-L. Lien, Treatment of chlorinated organic contaminants
622 with nanoscale bimetallic particles, Catal. Today 40 (1998) 387–395.
- 623 [25] R.W. Gillham, Discussion of Papers/Discussion of nano-scale iron for dehalogenation.
624 by Evan K. Nyer and David B. Vance (2001), Ground Water Monitoring &
625 Remediation, v. 21, no. 2, pages 41–54, Ground Water Monit. Remed 23 (2003) 6–8.
- 626 [26] W.-x. Zhang, Nanoscale iron particles for environmental remediation: an overview, J.
627 Nanopart. Res. 5 (2003) 323–332.
- 628 [27] X.Q. Li, D.W. Elliott, W.X. Zhang, Zero-valent iron nanoparticles for abatement of
629 environmental pollutants: materials and engineering aspects, Crit. Rev. Solid State
630 Mater. Sci. 31 (2006) 111–122.
- 631 [28] C. Macé, Controlling groundwater VOCs: do nanoscale ZVI particles have any
632 advantages over microscale ZVI or BNP? Pollut. Eng. 38 (2006) 24–27.
- 633 [29] C. Macé, S. Desrocher, F. Gheorghiu, A. Kane, M. Pupeza, M. Cernik, P. Kvapil, R.
634 Venkatakrishnan, W.-X. Zhang, Nanotechnology and groundwater remediation: A step
635 forward in technology understanding, Remed. J. 16 (2006) 23–33.
- 636 [30] P.G. Tratnyek, R.L. Johnson, Nanotechnologies for environmental cleanup, Nano Today
637 1 (2006) 44–48.
- 638 [31] T. Pradeep, Anshup, Noble metal nanoparticles for water purification: A critical review,
639 Thin Solid Films 517 (2009) 6441–6478.

- [32] A. Agarwal, H. Joshi, Environmental sciences application of nanotechnology in the remediation of contaminated groundwater: A short review, *Recent Res. Sci. Technol.* 2 (2010) 51–57.
- [33] N. Müller, B. Nowack, Nano zero valent iron – THE solution for water and soil remediation?. Report of workshop held in Zurich (Switzerland), November 24th 2009 (2010). http://www.observatorynano.eu/project/filesystem/files/nZVI_final_vsObservatory.pdf. (Access 2011/04/24)
- [34] C. Noubactep, S. Caré, On nanoscale metallic iron for groundwater remediation, *J. Hazard. Mater.* 182 (2010) 923–927.
- [35] L.G. Cullen, E.L. Tilston, G.R. Mitchell, C.D. Collins, L.J. Shaw, Assessing the impact of nano- and micro-scale zerovalent iron particles on soil microbial activities: Particle reactivity interferes with assay conditions and interpretation of genuine microbial effects, *Chemosphere* 82 (2011) 1675–1682.
- [36] C. Noubactep, Comment on “Reductive dechlorination of g-hexachloro-cyclohexane using Fe–Pd bimetallic nanoparticles” by Nagpal et al. [*J. Hazard. Mater.* 175 (2010) 680–687], *J. Hazard. Mater.* (2011) doi:10.1016/j.jhazmat.2011.03.081.
- [37] J.R. Peralta-Videa, L. Zhao, M.L. Lopez-Moreno, G. de la Rosa, J. Hong, J.L. Gardea-Torresdey, Nanomaterials and the environment: A review for the biennium 2008–2010, *J. Hazard. Mater.* 186 (2011) 1–15.
- [38] Z. Shi, J.T. Nurmi, P.G. Tratnyek, Effects of nano zero-valent iron on oxidation-reduction potential, *Environ. Sci. Technol.* 45 (2011) 1586–1592.
- [39] M.J. Truex, V.R. Vermeul, D.P. Mendoza, B.G. Fritz, R.D. Mackley, M. Oostrom, T.W. Wietsma, T.W. Macbeth, Injection of zero-valent iron into an unconfined aquifer using shear-thinning fluids, *Ground Water Monit. Remed.* 31 (2011) 50–58.
- [40] M.J. Truex, T.W. Macbeth, V.R. Vermeul, B.G. Fritz, D.P. Mendoza, R.D. Mackley, T.W. Wietsma, G. Sandberg, T. Powell, J. Powers, E. Pitre, M. Michalsen, S.J. Ballock-Dixon, L. Zhong, M. Oostrom, Demonstration of combined zero-valent iron and

- electrical resistance heating for in situ trichloroethene remediation. *Environ. Sci. Technol.* (2011) doi: 10.1021/es104266a.
- [41] T. Masciangioli, W.X. Zhang, Environmental technologies at the Nanoscale, *Environ. Sci. Technol.* 37 (2003) 102A–108A.
- [42] A. Ghauch, A. Tuqan, H. Abou Assi, Antibiotic removal from water: Elimination of amoxicillin and ampicillin by microscale and nanoscale iron particles, *Environ. Pollut.* 157 (2009) 1626–1635.
- [43] N. Sakulchaicharoen, D.M. O'Carroll, J.E. Herrera, Enhanced stability and dechlorination activity of pre-synthesis stabilized nanoscale FePd particles, *J. Contam. Hydrol.* 118 (2010) 117–127.
- [44] V. Nagpal, A.D. Bokare, R.C. Chikate, C.V. Rode, K.M. Paknikar, Reply to comment on “Reductive dechlorination of γ -hexachlorocyclohexane using Fe–Pd bimetallic nanoparticles”, by C. Noubactep, *J. Hazard. Mater.* (2011) doi:10.1016/j.jhazmat.2011.04.015.
- [45] C. Anstice, C. Alonso, F.J. Molina, Cover cracking as a function of bar corrosion: part I-experimental test, *Materials and structures* 26 (1993) 453–464.
- [46] S. Caré, Q.T. Nguyen, V. L'Hostis, Y. Berthaud, Mechanical properties of the rust layer induced by impressed current method in reinforced mortar, *Cement Concrete Res.* 38 (2008) 1079–1091.
- [47] Y. Zhao, H. Ren, H. Dai, W. Jin, Composition and expansion coefficient of rust based on X-ray diffraction and thermal analysis, *Corros. Sci.* 53 (2011) 1646–1658.
- [48] K.D. Grieger, A. Fjordboge, N.B. Hartmann, E. Eriksson, P.L. Bjerg, A. Baun, Environmental benefits and risks of zero-valent iron nanoparticles (nZVI) for in situ remediation: Risk mitigation or trade-off? *J. Contam. Hydrol.* 118 (2010) 165–183.

- [49] R.J. Barnes, C. J. van der Gast, O. Riba, L.E. Lehtovirta, J.I. Prosser, P.J. Dobson, I.P. Thompson, The impact of zero-valent iron nanoparticles on a river water bacterial community, *J. Hazard. Mater.* 184 (2010) 73–80.
- [50] M. Diao, M. Yao, Use of zero-valent iron nanoparticles in inactivating microbes, *Water Res.* 43 (2009) 5243–5251.
- [51] T. Tervonen, I. Linkov, J.R. Figueira, J. Steevens, M. Chappell, M. Merad, Risk-based classification system of nanomaterials, *J. Nanopart. Res.* 11 (2009) 757–766.
- [52] C. Noubactep (2007): Processes of contaminant removal in “Fe⁰–H₂O” systems revisited. The importance of co-precipitation, *Open Environ. J.* 1, 9–13.
- [53] C. Noubactep A critical review on the mechanism of contaminant removal in Fe⁰–H₂O systems, *Environ. Technol.* 29 (2008) 909–920.
- [54] C. Noubactep, The fundamental mechanism of aqueous contaminant removal by metallic iron, *Water SA* 36 (2010) 663–670.
- [55] M.I. Litter, M.E. Morgada, J. Bundschuh, Possible treatments for arsenic removal in Latin American waters for human consumption, *Environ. Pollut.* 158 (2010) 1105–1118.
- [56] R.A. Crane, M. Dickinson, I.C. Popescu, T.B. Scott, Magnetite and zero-valent iron nanoparticles for the remediation of uranium contaminated environmental water, *Water Res.* 45 (2011) 2931–2942.
- [57] O. Celebi, C. Uzum, T. Shahwan, H.N. Erten, A radiotracer study of the adsorption behavior of aqueous Ba²⁺ ions on nanoparticles of zero-valent iron, *J. Hazard. Mater.* 148 (2007) 761–767.
- [58] X.Q. Li, W.X. Zhang, Sequestration of metal cations with zerovalent iron nanoparticles—a study with high resolution X-ray photoelectron spectroscopy (HR-XPS), *J. Phys. Chem. C* 111 (2007) 6939–6946.

714 [59] H.K. Boparai, M. Joseph, D.M. O'Carroll, Kinetics and thermodynamics of cadmium ion
 715 removal by adsorption onto nano zerovalent iron particles, *J. Hazard. Mater.* 186 (2011)
 716 458–465.

717 [60] S. Xiao, H. Ma, M. Shen, S. Wang, Q. Huang, X. Shi, Excellent copper(II) removal using
 718 zero-valent iron nanoparticle - immobilized hybrid electrospun polymer nanofibrous
 719 mats, *Colloids Surf. A: Physicochem. Eng. Aspects* 381 (2011) 48–54.

720 [61] E.J. Reardon, R. Fagan, J.L. Vogan, A. Przepiora, Anaerobic corrosion reaction kinetics
 721 of nanosized iron, *Environ. Sci. Technol.* 42 (2008) 2420–2425.

722 [62] M. Stratmann, J. Müller, The mechanism of the oxygen reduction on rust-covered metal
 723 substrates, *Corros. Sci.* 36 (1994) 327–359.

724 [63] C. Noubactep, T. Licha, T.B. Scott, M. Fall, M. Sauter, Exploring the influence of
 725 operational parameters on the reactivity of elemental iron materials, *J. Hazard. Mater.*
 726 172 (2009) 943–951.

727 [64] S.H. Behrens, D.I. Christl, R. Emmerzael, P. Schurtenberger, M. Borkovec, Charging
 728 and aggregation properties of carboxyl latex particles: experiments versus DLVO
 729 theory, *Langmuir* 21 (2000) 2566–2575.

730 [65] M. Dickinson, T.B. Scott, The application of zero-valent iron nanoparticles for the
 731 remediation of a uranium-contaminated waste effluent, *J. Hazard. Mater.* 178 (2010)
 732 171–179.

733 [66] R.L. Johnson, R.B. Thoms, R.O.B. Johnson, J. Nurmi, P.G. Tratnyek, Mineral
 734 precipitation upgradient from a zero-valent iron permeable reactive barrier, *Ground*
 735 *Water Monit. Rem.* 28 (2008) 56–64.

736 [67] Y. Wu, J. Zhang, Y. Tong, X. Xu, Chromium (VI) reduction in aqueous solutions by
 737 Fe₃O₄-stabilized Fe⁰ nanoparticles, *J. Hazard. Mater.* 172 (2009) 1640–1645.

738 [68] Z. Fang, X. Qiu, J. Chen, X. Qiu, Degradation of the polybrominated diphenyl ethers by
739 nanoscale zero-valent metallic particles prepared from steel pickling waste liquor,
740 Desalination 267 (2011) 34–41.

741 [69] Z.LvL. Jiang, W. Zhang, Q. Du, B. Pan, L. Yang, Q. Zhang, Nitrate reduction using
742 nanosized zero-valent iron supported by polystyrene resins: Role of surface functional
743 groups. Water Res. 45 (2011) 2191–2198.

744 [70] M. Tong, S. Yuan, H. Long, M. Zheng, L. Wang, J. Chen, Reduction of nitrobenzene in
745 groundwater by iron nanoparticles immobilized in PEG/nylon membrane, J. Contam.
746 Hydrol. 122 (2011) 16–25.

747 [71] S. Yuan, Z. Zheng, X.-Z. Meng, J. Chen, L. Wang, Surfactant mediated HCB
748 dechlorination in contaminated soils and sediments by micro and nanoscale Cu/Fe
749 Particles. Geoderma 159 (2010) 165–173.

750 [72] N. Zhu, H. Luan, S. Yuan, J. Chen, X. Wu, L. Wang, Effective dechlorination of HCB by
751 nanoscale Cu/Fe particles. J. Hazard. Mater. 176 (2010), 1101–1105.

752 [73] B.S. Kadu, Y.D. Sathe, A.B. Ingle, R.C. Chikate, K.R. Patil, C.V. Rode, Efficiency and
753 recycling capability of montmorillonite supported Fe–Ni bimetallic nanocomposites
754 towards hexavalent chromium remediation, Appl. Catal. B: Environ. 104 (2011) 407–
755 414.

756 [74] C. Noubactep, S. Caré, F. Togue-Kamga, A. Schöner, P. Woaf, Extending service life
757 of household water filters by mixing metallic iron with sand, Clean – Soil, Air, Water 38
758 (2010) 951–959.

759 [75] V. Tarvainen, A. Ranta-Maunus, A. Hanhijärvi, H. Forsén, The effect of drying and
760 storage conditions on case hardening of scots pine and norway spruce timber, Maderas.
761 Ciencia y tecnología 8 (2006) 3–14.

- 762 [76] W.J.N. Fernando, A.L. Ahmad, S.R. Abd. Shukor, Y.H. Lok, A model for constant
763 temperature drying rates of case hardened slices of papaya and garlic, *J. Food Eng.* 88
764 (2008) 229–238
- 765 [77] Y. Zhuang, S. Ahn, A.L. Seyfferth, Y. Masue-Slowey, S. Fendorf, R.G. Luthy,
766 Dehalogenation of polybrominated diphenyl ethers and polychlorinated biphenyl by
767 bimetallic, impregnated, and nanoscale zerovalent iron, *Environ. Sci. Technol.* 45
768 (2011) 4896–4903.
- 769 [78] N. Moraci, P.S. Calabrò, Heavy metals removal and hydraulic performance in zero-
770 valent iron/pumice permeable reactive barriers, *J. Environ. Manag.* 91 (2010) 2336–
771 2341.
- 772 [79] Y.N. Vodyanitskii, The role of iron in the fixation of heavy metals and metalloids in
773 soils: a review of publications, *Eurasian Soil Sci.* 43 (2010) 519–532.
- 774 [80] S.R. Kanel, J.-M. Greneche, H. Choi, Arsenic(V) Removal from groundwater using nano
775 scale zero-valent iron as a colloidal reactive barrier material, *Environ. Sci. Technol.* 40
776 (2006) 2045–2050.
- 777 [81] D.D.J. Antia, Modification of aquifer pore-water by static diffusion using nano-zero-
778 valent metals. *Water* 3 (2011) 79–112.
- 779 [82] M. Flury, H. Flühler, Brilliant Blue FCF as a dye tracer for solute transport studies. A
780 toxicological review, *J. Environ. Qual.* 23 (1994) 1108–1112.
- 781 [83] A.E. Fryar, F.W. Schwartz, Hydraulic-conductivity reduction, reaction-front propagation,
782 and preferential flow within a model reactive barrier, *J. Contam. Hydrol.* 32 (1998) 333–
783 351.
- 784 [84] J. Simunek, N.J. Jarvis, M.T. van Genuchten, A. Gardenas, Review and comparison of
785 models for describing non-equilibrium and preferential flow and transport in the vadose
786 zone, *J. Hydrol.* 272 (2003) 14–35.

787 [85] B.E. Clothier, S.R. Green, M. Deurer, Preferential flow and transport in soil: progress
788 and prognosis, *Eur. J. Soil Sci.* 59 (2008) 2–13.

789 [86] S.E. Allaire, S. Roulier, A.J. Cessna, Quantifying preferential flow in soils: A review of
790 different techniques, *J. Hydrol.* 378 (2009) 179–204.

791 [87] D.C. McMurty, R.O. Elton, New approach to in-situ treatment of contaminated
792 groundwaters, *Environ. Progr.* 4/3 (1985) 168–170.

793 [88] M.D. Mackay, J.A. Cherry, Groundwater contamination: Pump-and-treat remediation,
794 *Environ. Sci. Technol.* 23 (1989) 630–636.

795 [89] R.C. Starr, J.A. Cherry, In situ remediation of contaminated Ground water: The funnel-
796 and-Gate System, *Ground Water* 32 (1994) 465–476.

797 [90] M. Min, H. Xu, J. Chen, M. Fayek, Evidence of uranium biomineralization in sandstone-
798 hosted roll-front uranium deposits, northwestern China, *Ore Geol. Rev.* 26 (2005) 198–
799 206.

800 [91] M. Sidborn, I. Neretnieks, Long term redox evolution in granitic rocks: Modelling the
801 redox front propagation in the rock matrix, *Appl. Geochem.* 22 (2007) 2381–2396.

802 [92] B. Gu, T.J. Phelps, L. Liang, M.J. Dickey, Y. Roh, B.L. Kinsall, A.V. Palumbo, G.K.
803 Jacobs, Biogeochemical dynamics in zerovalent iron columns: implications for
804 permeable reactive barriers, *Environ. Sci. Technol.* 33 (1999) 2170–2177.

805 [93] C. Su, R.W. Puls, Arsenate and arsenite removal by zerovalent iron: kinetics, redox
806 transformation, and implications for in situ groundwater remediation, *Environ. Sci.*
807 *Technol.* 35 (2001) 4562–4568.

808 [94] Y. Furukawa, J.-W. Kim, J. Watkins, R.T. Wilkin, Formation of ferrihydrite and
809 associated iron corrosion products in permeable reactive barriers of zerovalent iron,
810 *Environ. Sci. Technol.* 36 (2002) 5469–5475.

- 811 [95] T. Kohn, J.T. Kenneth, A. Livi, A.L. Roberts, P.J. Vikesland, Longevity of granular iron
812 in groundwater treatment processes: corrosion product development, *Environ. Sci.*
813 *Technol.* 39 (2005) 2867–2879.
- 814 [96] C.D. Palmer, P.R. Wittbrodt, Processes affecting the remediation of chromium-
815 contaminated sites, *Environ. Health Perspect.* 92 (1991) 25–40.
- 816 [97] S. Nesic, Key issues related to modelling of internal corrosion of oil and gas pipelines –
817 A review, *Corros. Sci.* 49 (2007) 4308–4338.
- 818 [98] J.R. Kiser, Bruce A. Manning, Reduction and immobilization of chromium(VI) by
819 iron(II)-treated faujasite. *J. Hazard. Mater.* 174 (2010) 167–174.
- 820 [99] M.J. Lottering, L. Lorenzen, N.S. Phala, J.T. Smit, G.A.C. Schalkwyk, Mineralogy and
821 uranium leaching response of low grade South African ores, *Miner. Eng.* 21 (2008) 16–
822 22.
- 823 [100] Y. Jiao, C. Qiu, L. Huang, K. Wu, H. Ma, S. Chen, L. Ma, L. Wu, Reductive
824 dechlorination of carbon tetrachloride by zero-valent iron and related iron corrosion,
825 *Appl. Catal. B: Environ.* 91 (2009) 434–440.
- 826 [101] R.J. Crawford, I.H. Harding, D.E. Mainwaring, Adsorption and coprecipitation of single
827 heavy metal ions onto the hydrated oxides of iron and chromium, *Langmuir* 9 (1993)
828 3050–3056.
- 829 [102] R.J. Crawford, I.H. Harding, D.E. Mainwaring, Adsorption and coprecipitation of
830 multiple heavy metal ions onto the hydrated oxides of iron and chromium, *Langmuir* 9
831 (1993) 3057–3062.
- 832 [103] K. Eusterhues, T. Rennert, H. Knicker, I. Kgel-Knabner, K.U. Totsche, U.
833 Schwertmann, Fractionation of organic matter due to reaction with ferrihydrite:
834 Coprecipitation versus adsorption, *Environ. Sci. Technol.* 45 (2011) 527–533.

835 [104] W.P. Johnson, H. Ma, E. Pazmino, Straining credibility: A general comment regarding
836 common arguments used to infer straining as the mechanism of colloid retention in
837 porous media, *Environ. Sci. Technol.* 45 (2011) 3831–3832.

838 [105] M. Kalin, W.N. Wheeler, G. Meinrath, The removal of uranium from mining waste
839 water using algal/microbial biomass, *J. Environ. Radioact.* 78 (2005) 151–177.

840 [106] C. Noubactep, Metallic iron for safe drinking water worldwide, *Chem. Eng. J.* 165
841 (2010) 740–749.

842 [107] D. Pokhrel, T. Viraraghavan, Arsenic removal in an iron oxide-coated fungal biomass
843 column: Analysis of breakthrough curves, *Biores. Technol.* 99 (2008) 2067–2071.

844 [108] D. Pokhrel, B.S. Bhandari, T. Viraraghavan, Arsenic contamination of groundwater in
845 the Terai region of Nepal: an overview of health concerns and treatment options,
846 *Environ. Int.* 35 (2009) 157–161.

847 [109] D. Pokhrel, T. Viraraghavan, Biological filtration for removal of arsenic from drinking
848 water, *J. Environ. Manage.* 90 (2009) 1956–1961.

849 [110] J.S. Morrison, R.R. Sprangler, Chemical barriers for controlling groundwater
850 contamination, *Environ. Progr.* 12 (1993) 175–181.

851 [111] J.S. Morrison, R.R. Sprangler, S.A. Morris, Subsurface injection of dissolved ferric
852 chloride to form a chemical barrier: Laboratory investigations, *Ground Water* 34 (1996)
853 75–83.

854 [112] K. Hanna, J.-F. Boily, Sorption of two naphthoic acids to goethite surface under flow
855 through conditions, *Environ. Sci. Technol.* 44 (2010) 8863–8869.

856 [113] A. Ghauch, H. Abou Assi, S. Bdeir Aqueous removal of diclofenac by plated elemental
857 iron: Bimetallic systems, *J. Hazard. Mater.* 182 (2010) 64–74.

858 [114] C. Noubactep, Aqueous contaminant removal by metallic iron: Is the paradigm shifting?
859 *Water SA* 37 (2011) xy–zt.

- 860 [115] R.L. Reynolds, M.B. Goldhaber, Origin of a south Texas roll-type uranium deposit: I.
861 Alteration of iron-titanium oxide minerals, *Econ. Geol.* 73 (1978) 1677–1689.
- 862 [116] J. Posey-Dowty, E. Axtmann, D. Crerar, M. Borcsik, A. Ronk, W. Woods, Dissolution
863 rate of uraninite and uranium roll-front ores. *Econ. Geol.* 82 (1987) 184–194.
- 864 [117] L. Romero, I. Neretnieks, L. Moreno, Movement of the redox front at the Osamu
865 Utsumi uranium mine, Poços de Caldas, Brazil, *J. Geochem. Explor.* 45 (1992) 471–
866 501.
- 867 [118] D. Read, T.A. Lawless, R.J. Sims, K.R. Butter, Uranium migration through intact
868 sandstone cores, *J. Cont. Hydrol.*, 13 (1993) 277–289.
- 869

Table 1: Results of a web-search in 7 selected relevant journals demonstrating the current interest within academia for the nano-Fe⁰ technology.

Journal	Impact	Issues	Search's results		
	Factor	(year ⁻¹)	Period	Total	2011
Environ. Sci. Technol.	4.630	24	1995 to 2011	157	13
J. Hazard. Mater.	4.144	33	2004 to 2011	86	15
Chemosphere	3.253	44	2000 to 2011	49	5
Water Res.	4.355	20	2005 to 2011	31	9
Chem. Eng. J.	2.816	30	2008 to 2011	15	6
Desalination	2.034	48	2008 to 2011	12	9
Environ. Pollut.	3.426	12	2007 to 2011	12	1
Appl. Catal. B	5.252	32	2009 to 2011	3	1
Total				365	59

875 **Table 2:** Relevant redox couples for the process of aqueous Fe^0 dissolution and oxide scale
876 formation in a passive remediation $\text{Fe}^0/\text{H}_2\text{O}$ system. These processes are thermodynamically
877 the same for all Fe^0 particle sizes. Observed differences are due to kinetics aspects.
878

Electrode reactions			Eq.
Fe^0	\Leftrightarrow	$\text{Fe}^{2+} + 2 \text{e}^-$	(1)
Oxic conditions			
$\text{O}_2 + 2 \text{H}_2\text{O} + 4 \text{e}^-$	\Leftrightarrow	4OH^-	(2a)
$2 \text{H}_2\text{O} + 2 \text{e}^-$	\Leftrightarrow	$\text{H}_2 + 2 \text{OH}^-$	(2b)
Anoxic conditions			
$\text{O}_2 + 4 \text{H}^+ + 4 \text{e}^-$	\Leftrightarrow	$2 \text{H}_2\text{O}$	(3a)
$2 \text{H}^+ + 2 \text{e}^-$	\Leftrightarrow	H_2	(3b)

879

Table 3: Summary of the values of the number of particles contained in 1 kg of each material, the number of layer making up each particle and estimation of the relative time (τ). The life span of nano-Fe⁰ is operationally considered as the unit of time while assuming uniform corrosion. τ coincides with the ratio of the number of layers of Fe in each particle to that of nano-Fe⁰. The ratio of the number of particles in individual systems is also given.

Size	d	n _{particles}	n _{layers}	n _{layers} /n _{nano}	n _{nano} /n _{particles}	τ
	(μm)	(-)	(-)	(-)	(-)	(-)
Nano-Fe⁰	25*10 ⁻³	1.96*10 ¹⁸	87.2	1.0	1.0	1.0
$\mu\text{m-Fe}^0$	25	1.96*10 ⁹	87.2*10 ³	10 ³	10 ⁹	10 ³
mm-Fe⁰	250	1.96*10 ⁶	87.2*10 ⁴	10 ⁴	10 ¹²	10 ⁴
mm-Fe⁰	1000	3.06*10 ⁴	3.49*10 ⁵	4*10 ⁴	6.4*10 ¹³	4*10 ⁴

Table 4: Estimation of the value of the life span (t_{∞}) of a nano-Fe⁰ particle with 25 nm diameter for barrier life spans (t) from 10 to 40 years. The considered conventional reactive wall contains granular Fe⁰ with a diameter of 1 mm. For comparison the relative life span (in days and years) of the micrometric particles is given.

t	(years)	5	10	15	20	25	30	35	40
$t_{\mu\text{m}}$	(days)	45.7	91.3	137.0	182.6	228.3	273.9	319.6	365.3
$t_{\mu\text{m}}$	(years)	0.2	0.3	0.5	0.7	0.9	1.0	1.2	1.4
t_{∞}	(hours)	1.1	2.2	3.3	4.4	5.5	6.6	7.7	8.8

Table 5: Estimation of the extent of porosity loss (ΔV) due to the volumetric expansion of iron corrosion for Fe^0 particles of different sizes. The operational unit of time is arbitrarily the time to nano- Fe^0 depletion (t_∞). V_0 is the volume occupied by the initial Fe^0 particles; V_∞ is the volume occupied by residual Fe^0 and in-situ formed corrosion products. ΔV corresponds to the volume of pore occupied by the volumetric expansion of corrosion products. m_{consumed} = mass of Fe^0 consumed; v = percent of Fe^0 depletion, $n_{\text{Fe(II)}}$ = number of moles of corroded Fe^0 ; $n_{\text{Fe}_3\text{O}_4}$ = number of moles of generated iron corrosion products, $n_{\text{electrons}} = 2 * n_{\text{Fe(II)}}$ = number of electrons released by corroded iron; and $n_{\text{nano}}/n_{\text{electrons}}$ is the ratio of the number of electrons produced in by nano- Fe^0 to $n_{\text{electrons}}$.

Size	m_{consumed}	v	V_∞	ΔV	ΔV	$n_{\text{Fe(II)}}$	$n_{\text{Fe}_3\text{O}_4}$	$n_{\text{electrons}}$	$n_{\text{nano}}/n_{\text{electrons}}$
	(kg)	(%)	(mL)	(mL)	(%)	(moles)	(moles)	(moles)	(-)
nm- Fe^0	10^0	100.00	264.16	137.16	108.00	17.857	5.9524	35.714	1
μm - Fe^0	$3 * 10^{-3}$	0.30	127.41	0.41	0.32	0.053	0.0178	0.107	335
mm- Fe^0	$3 * 10^{-4}$	0.03	127.04	0.04	0.03	0.005	0.0018	0.011	3342
mm- Fe^0	$7.5 * 10^{-5}$	0.01	127.01	0.01	0.01	0.001	0.0004	0.003	13369

Table 6: Summary of the values of the number of particles contained in 1 kg of each nano- Fe^0 , the number of layer making up each particle and estimation of the relative time (τ). The life span of the material with the smallest particle size ($d = 10$ nm) is operationally considered as the unit of time while assuming uniform corrosion. The ratio of the number of particles in 1 kg of $d = 10$ nm to that of other d values is also given.

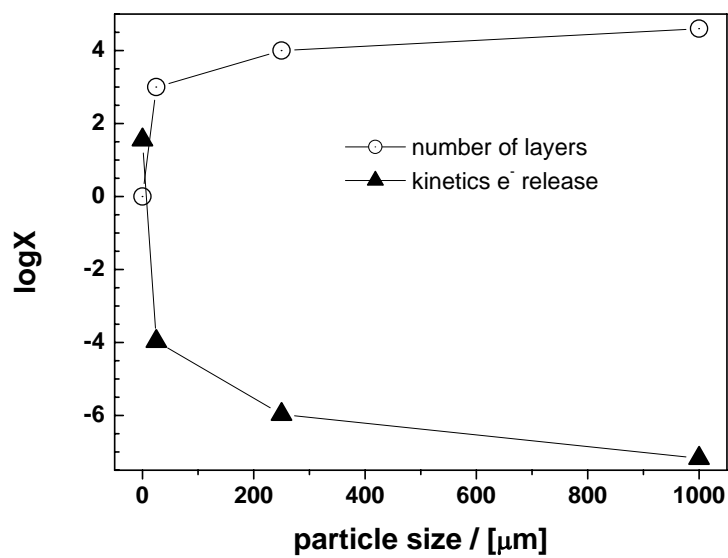
d	n_{particles}	n_{layers}	n_{layers}/n₁₀	n₁₀/n_{particles}	τ
(nm)	(-)	(-)	(-)	(-)	(-)
10	3.06×10^{19}	34.9	1.0	1.0	1.0
25	1.96×10^{18}	87.2	2.5	16	2.5
50	2.45×10^{11}	174.5	5.0	125	5.0
75	7.25×10^{16}	261.7	7.5	422	7.5
100	3.06×10^{16}	348.9	10.0	1000	10.0

Table 7: Summary of the extent of porosity loss (ΔV_{pore} in %) as 1 kg of nano-Fe⁰ ($V_0 = 127$ mL) is corroded to various iron oxides. V_{∞} is the volume of iron oxide at Fe⁰ exhaustion. The initial volume of pore (V_{pore}) is 530.4 mL and V'_{pore} is the residual pore volume at Fe⁰ exhaustion. The absolute value of negative values for V'_{pore} corresponds to the mass of nano-Fe⁰ which can not oxidize because of lack of space for volumetric expansion.

Fe species	η	V_{∞}	ΔV	V'_{pore}	ΔV_{pore}
	(-)	(mL)	(mL)	(mL)	(%)
Fe ⁰	1	127	0	403.4	23.9
Fe ₃ O ₄	2.08	264.2	137.2	266.2	49.8
Fe ₂ O ₃	2.12	269.2	142.3	261.1	50.8
α -FeOOH	2.91	369.6	242.6	160.8	69.7
γ -FeOOH	3.03	384.8	258.0	145.6	72.6
β -FeOOH	3.48	442.0	315.0	88.4	83.3
Fe(OH) ₂	3.75	476.3	349.3	54.1	89.8
Fe(OH) ₃	4.2	533.4	406.4	-3.0	100.0
Fe(OH) ₃ .3H ₂ O	6.4	812.8	685.8	-282.4	100.0

931 **Figure 1**

932



933

Figure 2

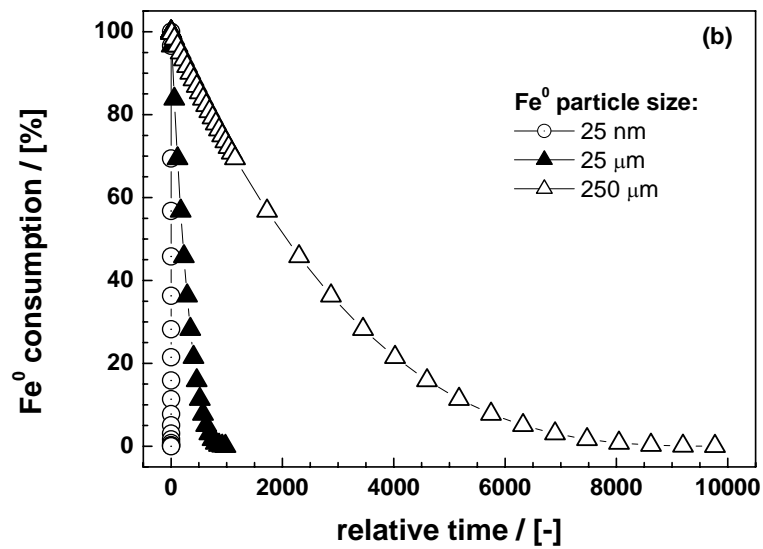
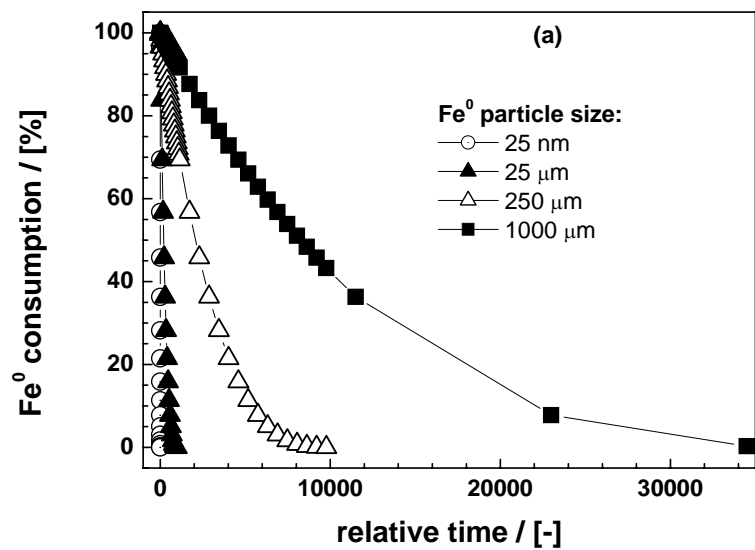


Figure 3

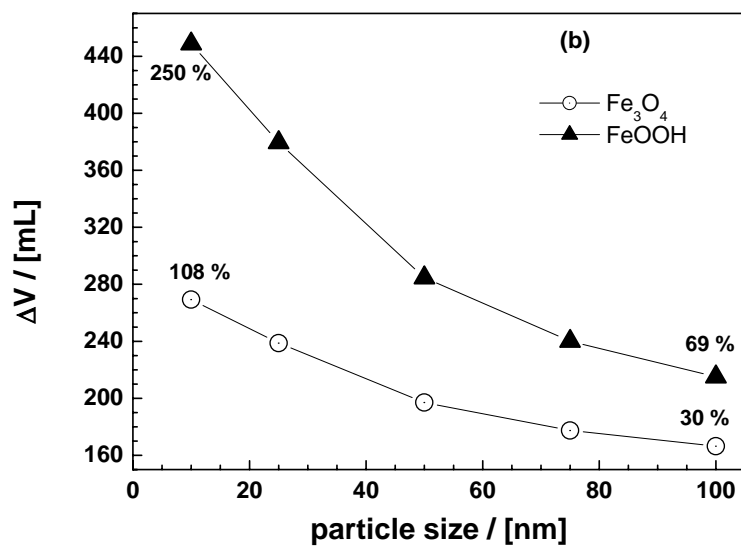
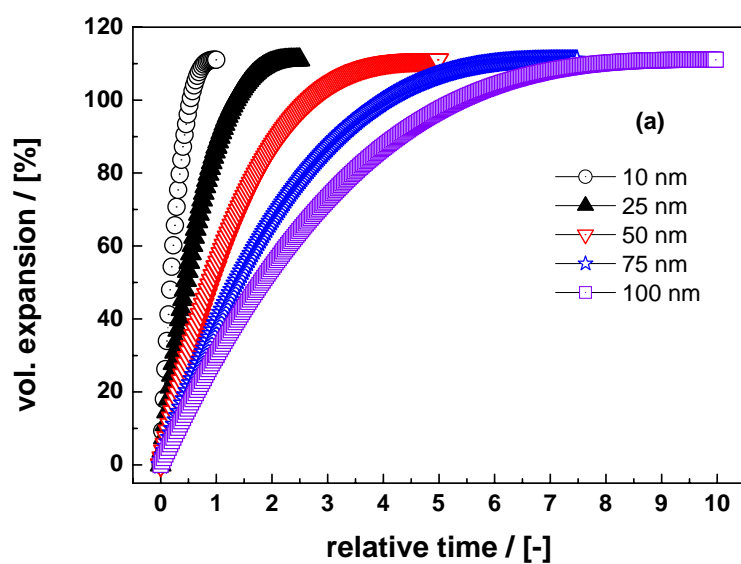
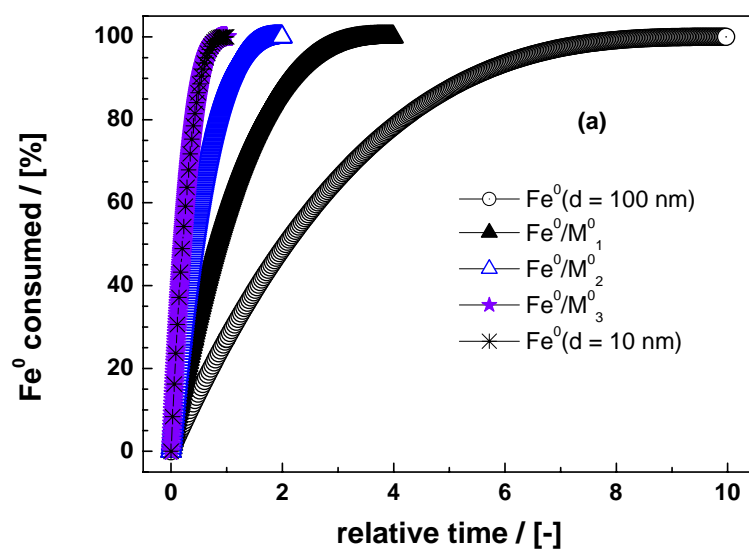


Figure 4:



951 **Figure 5**

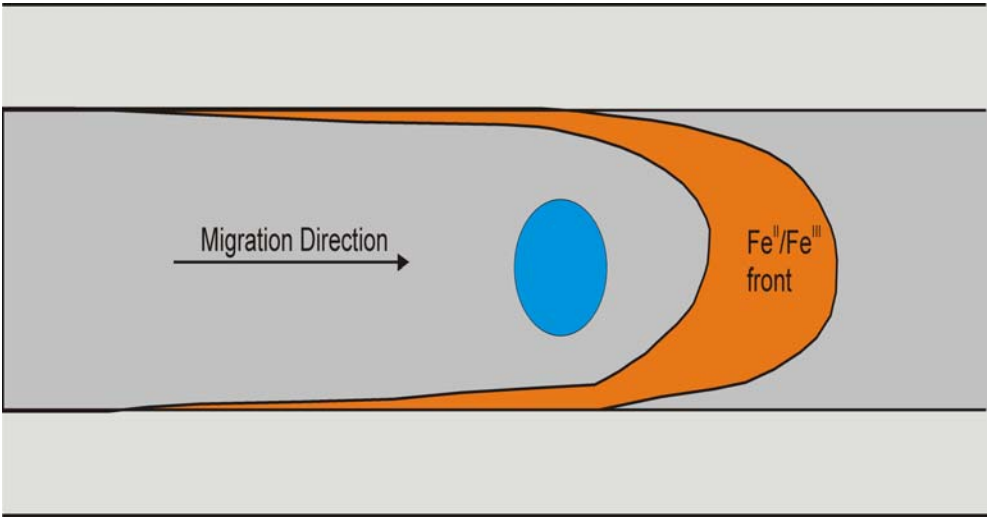
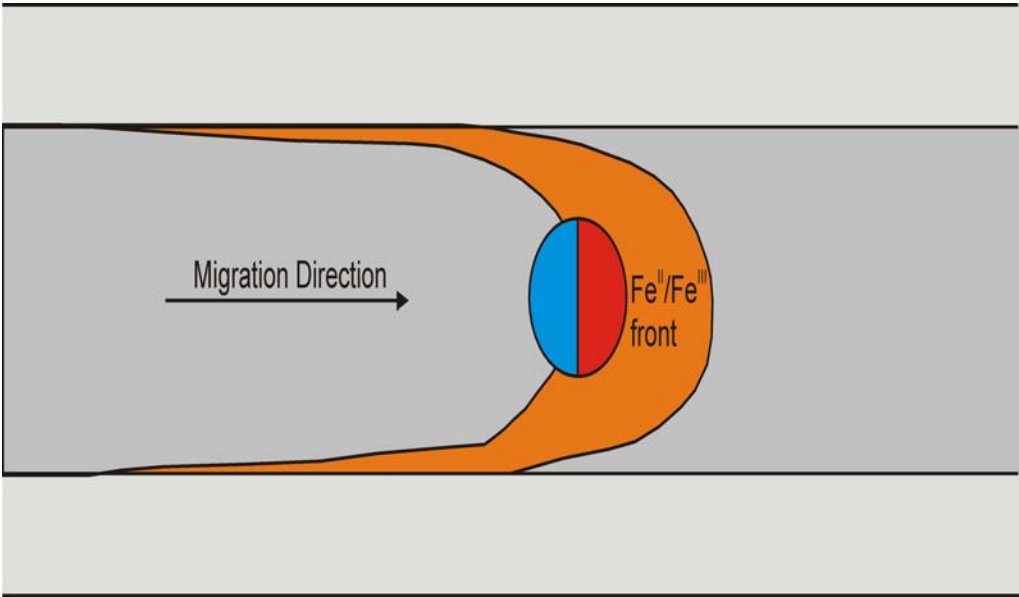
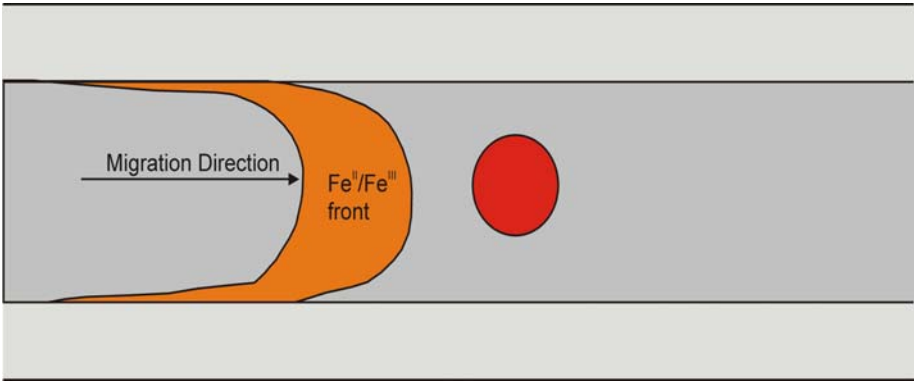


Figure captions

Figure 1: Comparison of the evolution of the kinetics of electron release and the number of layers in each Fe^0 particle as a function of the particle size. It is shown that smaller particles release huge amounts of electrons within a very short time. Calculations are made for 1 kg of Fe^0 material.

Figure 2: Kinetics of the process of Fe^0 exhaustion at nano-, micro- and millimetre scale as for: (a) $d \leq 1000 \mu\text{m}$, and (b) $d \leq 200 \mu\text{m}$.

Figure 3: Kinetics of the process of porosity loss at nano-scale as characterized by: (a) the percent volumetric expansion for the five considered particle sizes, and (b) the absolute value of ΔV (mL) at $\tau = 1$ for two different iron corrosion products (Fe_3O_4 and FeOOH).

Figure 4: Calculated extent of Fe^0 exhaustion as a function of the relative time (τ) for three ideal bimetallic systems based on the material with 100 nm diameter. The material with 10 nm diameter is represented for comparison.

Figure 5: Schematic diagram of the flow process of the U-shaped redox-front through a contaminated zone. Despite the relative importance of preferential flow paths, contaminants are “swept” by the roll-front.